CrossMark

An Extremely Metal-poor Lyα Emitter Candidate at $z = 6$ Revealed through Absorption Spectroscopy

Dominika Ďurovčíková[1,2] , Anna-Christina Eilers[1,2] , Robert A. Simcoe[1,2] , Louise Welsh[3,4] , Romain A. Meyer[5] ,
Jorryt Matthee[6] , Emma V. Ryan-Weber[7,8] , Minghao Yue[1] , Harley Katz[9,10] , Sindhu Satyavolu[11] , George Becker[12] ,
Frederick B. Davies[13] , and Emanuele Paolo Farina[14]

[1] MIT Kavli Institute for Astrophysics and Space Research, 77 Massachusetts Avenue, Cambridge, MA 02139, USA; dominika@mit.edu
[2] Department of Physics, Massachusetts Institute of Technology, 77 Massachusetts Avenue, Cambridge, MA 02139, USA
[3] Centre for Extragalactic Astronomy, Department of Physics, Durham University, South Road, Durham DH1 3LE, UK
[4] INAF—Osservatorio Astronomico di Trieste, via G. B. Tiepolo 11, I-34143 Trieste, Italy
[5] Department of Astronomy, University of Geneva, Chemin Pegasi 51, 1290 Versoix, Switzerland
[6] Institute of Science and Technology Austria (ISTA), Am Campus 1, A-3400 Klosterneuburg, Austria
[7] Centre for Astrophysics and Supercomputing, Swinburne University of Technology, Hawthorn, Victoria 3122, Australia
[8] AR. Centre of Excellence for All Sky Astrophysics in 3 Dimensions (ASTRO 3D), Australia
[9] Department of Astronomy & Astrophysics, University of Chicago, 5640 S Ellis Avenue, Chicago, IL 60637, USA
[10] Kavli Institute for Cosmological Physics, University of Chicago, Chicago, IL 60637, USA
[11] Institut de Física d'Altes Energies (IFAE), The Barcelona Institute of Science and Technology, Edifici Cn, Campus UAB, 08193, Bellaterra (Barcelona), Spain
[12] Department of Physics & Astronomy, University of California, Riverside, CA 92521, USA
[13] Max Planck Institut für Astronomie, Königstuhl 17, D-69117, Heidelberg, Germany
[14] International Gemini Observatory/NSF NOIRLab, 670 N A'ohoku Place, Hilo, HI 96720, USA

Abstract

We report the discovery of a Lyα emitter (LAE) candidate in the immediate foreground of the quasar PSO J158-14 at $z_{QSO} = 6.0685$ at a projected distance ~ 29 pkpc that is associated with an extremely metal-poor absorption system. This system was found in archival observations of the quasar field with the Very Large Telescope (VLT)/ Multi-Unit Spectroscopic Explorer (MUSE) and was previously missed in searches of absorption systems using quasar absorption line spectroscopy, as it imparts no detectable metal absorption lines on the background quasar spectrum. The detected Lyα emission line at a redshift of $z_{LAE} = 6.0323$ is well aligned with the outer edge of the quasar's proximity zone and can plausibly cause its observed damping wing if it is associated with a proximate subdamped Lyα absorption system with a column density of $\log N_{HI}/cm^{-2} \approx 19.7$. A >10 hr medium-resolution spectrum of the quasar observed with the Magellan/Folded-port InfraRed Echellette (FIRE) and VLT/X-Shooter spectrographs reveals a metallicity constraint of $[Z/H] < -3$. Such low metallicity makes this system an extremely metal-poor galaxy candidate and provides an exciting site to study possible signatures of Population III stars.

1. Introduction

Finding Population III (Pop III) stars is one of the most sought-after endeavors in modern astrophysics due to their important role in the formation of the first structures in the early Universe (e.g., R. S. Klessen & S. C. O. Glover 2023). Pop III stars are the first generation of stars that collapsed from pristine, (nearly) metal-free gas produced by the Big Bang nucleosynthesis. They are thought to create the first heavy elements, and their remnants possibly provide the initial seeds for the earliest supermassive black holes. Their direct detection remains elusive as the majority of Pop III stars are thought to have mostly formed early in the history of the Universe ($z \sim$ 20–30) and their likely heavy masses (e.g., T. Abel et al. 2002; V. Bromm 2017) caused them to have very short lifetimes ($\sim$a few Myr). Furthermore, they are thought to reside in minihalos (S. Hirano et al. 2015; A. T. P. Schauer et al. 2019) with luminosities that should be challenging to detect at such high

redshifts even with the sensitivity of the James Webb Space Telescope (JWST; A. T. P. Schauer et al. 2020).

Despite the challenges in directly detecting Pop III stars, significant progress has been made in studying their signatures indirectly through observational probes and theoretical modeling. Examples include the study of extremely metal-poor ($[Fe/H] < -3$) stars in the Local Group (Pop II; e.g., T. C. Beers & N. Christlieb 2005; A. Frebel & J. E. Norris 2015) or the imprints of Pop III stellar feedback on the largest scales (P. Madau & M. Dickinson 2014). Recently, substantial progress has been made on developing new optical emission-line diagnostics that could enable the study of this elusive stellar population in the early Universe (e.g., K. Nakajima & R. Maiolino 2022; H. Katz et al. 2023; H. Katz et al. 2024; I. Vanni et al. 2024). In fact, a handful of metal-poor systems at high redshift have already been identified through their emission-line properties (e.g., E. Vanzella et al. 2023; A. J. Cameron et al. 2024; R. Maiolino et al. 2024; F. Cullen et al. 2025; S. Fujimoto et al. 2025; R. P. Naidu et al. 2025), with metallicities as low as $12 + \log(O/H) < 6.3$, or $[O/H] < -2.4$ (E. Vanzella et al. 2023).

Theoretical models predict that pristine gas pockets and Pop III star formation can persist beyond $z \sim 6$ (L. Tornatore et al. 2007; J. L. Johnson & A. Aykutalp 2019). One method to
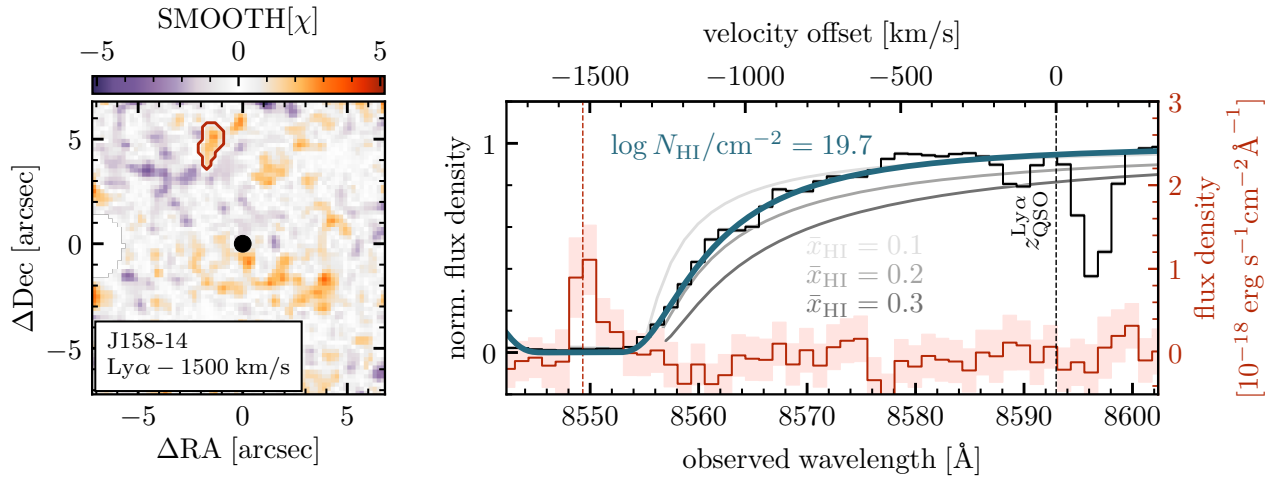
Figure 1. Left: a smoothed, point-spread function (PSF)-subtracted SNR image (SMOOTH[χ]) from MUSE showing the newly identified LAE in the foreground of the quasar PSO J158-14 (offset by -1500 km s^{-1} from the Lyα emission of the quasar). Right: the LAE spectrum from the original (not PSF-subtracted) MUSE data cube extracted over the contour shown in the left panel is shown in red (1σ and 2σ uncertainties shown as shaded red regions). The quasar spectrum is shown in black with gray uncertainties, which are too small to be clearly visible, with its Lyα redshift marked by $z_{\mathrm{QSO}}^{\mathrm{Ly}\alpha}$. The redshift of the LAE, $z_{\mathrm{LAE}}^{\mathrm{Ly}\alpha} = 6.0323$ aligns with the end of the quasar's proximity zone, and an absorber with a column density of log $N_{\mathrm{HI}}/\mathrm{cm}^{-2} \approx 19.7$ (a sub-DLA) can be used to model the damping wing of this quasar. For comparison, we also overplot example damping wing profiles arising from a homogenous IGM at a volume-averaged neutral gas fraction of $\bar{x}_{\mathrm{HI}} = 10\%$, 20%, and 30% (J. Miralda-Escudé 1998). Note that the quasar spectrum has been continuum normalized to enable damping wing modeling (see Section 2.2 for details), while the LAE spectrum is shown in absolute flux density units (red y-axis on the right). No other emission lines are seen across the wavelength range of MUSE.

search for such isolated environments is via absorption systems along sightlines to distant quasars (e.g., G. D. Becker et al. 2011, 2019; V. D'Odorico et al. 2022, 2023). Quasar absorption line spectroscopy has proven extremely useful in studying chemical enrichment across cosmic time (e.g., R. A. Simcoe et al. 2002; J. Schaye et al. 2003; E. V. Ryan-Weber et al. 2009; R. Cooke et al. 2011; R. L. Davies et al. 2023b; L. Welsh et al. 2024, refer to X. Fan et al. 2023 for a review), particularly through damped Lyα absorption systems (DLAs; log $N_{\mathrm{HI}}/\mathrm{cm}^{-2} > 20.3$). DLAs produce distinctive features in a quasar spectrum. The neutral hydrogen produces a saturated Voigt absorption line profile with a Lorentzian damping wing in the Lyα forest. This is accompanied by low-ionization metal absorption lines at the same redshift due to the metals present in the gas. More diffuse systems that are still optically thick to Lyα, such as Lyman limit systems and subdamped Lyα absorption systems (sub-DLAs) with $17.2 \leqslant$ log $N_{\mathrm{HI}}/\mathrm{cm}^{-2} \leqslant 20.3$, are of particular importance in searching for pristine, isolated environments as their densities are not sufficient to sustain star formation that would cause chemical enrichment by further generations of stars (M. Fumagalli et al. 2011; S. Salvadori & A. Ferrara 2012; M. Fumagalli et al. 2016; A. Saccardi et al. 2023).

At $z \gtrsim 5$, the increasingly neutral intergalactic medium (IGM) suppresses the Lyα forest and renders identifying absorption systems therein significantly more challenging (e.g., J. E. Gunn & B. A. Peterson 1965; R. A. Simcoe et al. 2020; X. Fan et al. 2023). Searches for such high-redshift H I-rich gas clouds are thus mostly restricted to cases where the absorber lies in the region of increased flux transmission in the immediate foreground of the quasar, known as the proximity zone (e.g., R. Cen & Z. Haiman 2000, P. Madau & M. J. Rees 2000, Z. Haiman & R. Cen 2001, X. Fan et al. 2006; also note recent work doing this in galaxy sightlines by K. E. Heintz et al. 2025). Such systems have been found near a handful of high-redshift quasars as proximate DLAs (pDLAs; V. D'Odorico et al. 2018; E. Bañados et al. 2019; F. B. Davies et al. 2023a). Even then, disentangling the

quasar's Lyα damping wing due to the proximate absorber from the imprint of the neutral IGM has only been enabled through the detection of metal absorption lines in the quasar spectrum, which concurrently provide a valuable constraint on the metallicity of the intervening gas cloud (R. A. Simcoe et al. 2012; E. Bañados et al. 2019; F. Wang et al. 2020).

Given the required presence of metal absorption lines, the identified pDLAs near reionization-era quasars are not pristine anymore, as they already show significant metal enrichment (V. D'Odorico et al. 2018; E. Bañados et al. 2019). Therefore, to identify the most metal-poor systems that could potentially host Pop III stars, one has to look for proximate absorption systems in high-redshift quasar sightlines that do not produce strong associated metal line absorption. This is especially challenging during the epoch of reionization, as metal-poor proximate absorption systems can be easily confused with Lyα damping wings caused by the IGM. In this Letter, we report on the discovery of such a proximate absorption system in the field of a $z = 6$ quasar.

Throughout this Letter, we use the flat ΛCDM cosmology with $h = 0.67$, $\Omega_M = 0.31$, and $\Omega_\Lambda = 0.69$ (Planck Collaboration et al. 2020).

2. Evidence for a Metal-poor Absorption System in PSO J158-14

2.1. IGM Damping Wing or Absorption System?

The quasar PSO J158-14 at $z_{\mathrm{QSO}} = 6.0685$ (B. Chehade et al. 2018; A.-C. Eilers et al. 2020) exhibits a somewhat unexpected damping-wing-like Lyα transmission profile (Figure 1). All current constraints on the history of reionization (S. E. I. Bosman et al. 2018; A.-C. Eilers et al. 2018; J. Yang et al. 2020; S. E. I. Bosman et al. 2022; D. Ďurovčíková et al. 2024) imply a very low volume-averaged neutral gas fraction at this redshift ($\bar{x}_{\mathrm{HI}} \lesssim 0.2$), which makes seeing strong damping wings due to the IGM unlikely. There is growing evidence of neutral islands and damping wings persisting at $z < 6$ (G. D. Becker et al. 2024; B. Spina et al. 2024;
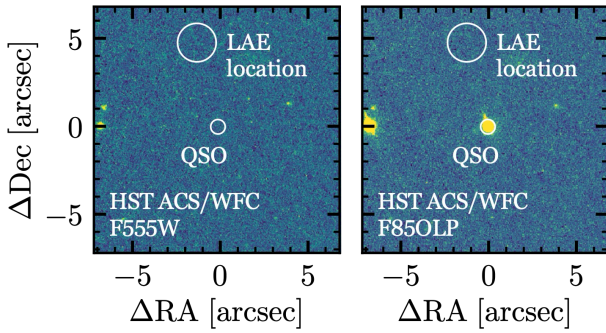
Figure 2. Archival imaging data of the quasar field from HST. Left: it is unlikely that this emission is not Lyα as no foreground emission is detected by HST ACS/WFC imaging with the F555W filter at a limiting magnitude of 26.88. Right: a nondetection in the F850LP filter at a limiting magnitude of 25.98 is consistent with the Lyα line flux measured in MUSE.

Y. Zhu et al. 2024; F. Sawyer et al. 2025) due to a patchy reionization topology; however, simulations have shown that the likelihood of PSO J158-14 having a damping wing due to our sightline randomly crossing a neutral patch in the IGM is <0.2% (S. Satyavolu et al. 2023). S. Satyavolu et al. (2023) also noticed weak extended flux just blueward of the proximity zone, indicating that this quasar's damping-wing-like absorption profile might in fact not be due to the IGM. Despite this fact, no metal absorption lines associated with a proximate absorption system have been found in the spectrum of this quasar (A.-C. Eilers et al. 2020; R. L. Davies et al. 2023b). This suggests that if a proximate absorber is the cause of the observed damping wing, it must be composed of metal-poor gas.

Using deep (~8.5 hr) observations with the Very Large Telescope/Multi-Unit Spectroscopic Explorer (VLT/MUSE; R. Bacon et al. 2010), we have identified a likely Lyα emitter (LAE) with an integrated line flux of $F_{Ly\alpha}^{LAE} \approx 2 \times 10^{-18}\,\mathrm{erg\,s^{-1}\,cm^{-2}}$ in the immediate foreground of the quasar PSO J158-14 at a transverse distance of ~5″ (~29 pkpc, with the coordinates of 10:34:46.6 −14:25:10.9; left panel of Figure 1). Note that the displayed pseudonarrowband image (SMOOTH[χ] is essentially a smoothed signal-to-noise image, following the definition of E. P. Farina et al. 2017), collapsed over a spectral width of 100 km s⁻¹, shows other patches of comparable signal-to-noise ratio (SNR); however, only the pixels marked by the LAE contour show a clear, isolated emission line structure in the velocity space. At the position of this LAE, we detect no other emission lines over the wavelength range of MUSE. We refer the reader to D. Ďurovčíková et al. (2025, in preparation) for details on the MUSE observations and data reduction, and here only note that the MUSE data were reduced using v2.8.7 of the MUSE Data Reduction Software (P. M. Weilbacher et al. 2012, 2014) with standard parameters.

In order to test whether the detected emission line could be from a lower-redshift galaxy, we inspected archival imaging data of this quasar field taken with the Advanced Camera for Surveys (ACS) on board the Hubble Space Telescope (HST; Proposal ID: 16756, PI: Eilers; previously analyzed by M. Yue et al. 2023). Neither of the two ~30 minute exposures, taken with the Wide Field Channel (WFC) F850LP and F555W filters, show a detection at the location of this LAE (Figure 2). A nondetection in the F850LP image (which has a 3σ limiting AB magnitude of 25.98 over the area of the LAE) is not surprising, as the line flux detected from MUSE would

correspond to a source with $m_{AB} \approx 29.9$ in this image. A nondetection of the LAE continuum further allows us to place a lower limit on the observed equivalent width of the Lyα line of $EW_{obs}(Ly\alpha) \gtrsim 33$ Å. A nondetection in the F555W image is also consistent with this emission line being Lyα at $z \sim 6$, as its foreground flux would be suppressed by the IGM. If this source were, however, a foreground interloper, the low-redshift galaxy would have to be fainter than 26.88 magnitude (which is the 3σ limiting AB magnitude over the LAE area).[15]

Thus, we assume that the detected line is indeed Lyα and the centroid of this emission line yields a redshift of $z_{LAE}^{Ly\alpha} = 6.0323$, which aligns with the spectral region where we would expect an associated absorption system to be placed, i.e., the outer edge of the quasar's observed proximity zone (right panel of Figure 1). Using a Voigt profile (shown in blue) and assuming the absorber to be at the same redshift as the LAE, we find that the observed absorption profile can indeed be modeled using a sub-DLA with an estimated H I column density of $\log N_{HI}/cm^{-2} \approx 19.7$, assuming the broadening parameter to be $b = 5\,km\,s^{-1}$. This value of b is in the range of typical values found in low-metallicity absorption systems (R. Cooke et al. 2011; L. Welsh et al. 2024; A. Sodini et al. 2024), even considering that linewidths tend to be narrower as metallicity decreases (e.g., C. Ledoux et al. 2006; M. T. Murphy et al. 2007). Note that the inferred H I column density and the subsequent results are not sensitive to the precise choice of b as long as $b \lesssim 50\,km\,s^{-1}$, and the final metallicity constraint is unchanged even if b is as low as $3\,km\,s^{-1}$.

2.2. Metallicity from Absorption Spectroscopy

To derive a metallicity constraint for this absorber, we obtain a high-SNR, medium-resolution spectrum of the quasar to search for associated metal absorption lines. We coadded archival, shallow VLT/X-Shooter (J. Vernet et al. 2011) observations of this quasar from 2017 January 24 (4320 s/1.2 hr; Program ID: 096.A-0418, PI: Shanks) with a newly observed deep spectrum taken with the Folded-port InfraRed Echellette (FIRE) spectrograph on the Magellan telescope (R. A. Simcoe et al. 2013). Magellan/FIRE observations come from 2023 January 13 (9600 s), 2024 July 14 (4800 s), and 2025 January 13 (18,000 s), totaling 9 hr of exposure time. These observations were reduced using the PypeIt package[16] (J. X. Prochaska et al. 2020b, 2020a), and we refer the reader to D. Ďurovčíková et al. (2024) for a more detailed description of the FIRE data reduction. The final spectrum, at a resolution of ~30 km s⁻¹, thus includes 10.2 hr of exposure time and is shown in the top part of Figure 3. Spectra from individual nights were calibrated to J_{AB} magnitude of 19.19 (J.-T. Schindler et al. 2020) before coadding to create the final spectrum displayed here.[17]

---

[15] Note that if the emission line detected in MUSE were Hα, this dwarf galaxy would be at $z = 0.3$ and its [O II]3727Å emission line would fall into the F555W filter. Additionally, Hβ and [O III] lines would fall into the wavelength range of MUSE, and could have been detected. Additionally, if the detected emission line were [O II]3727Å (corresponding to a galaxy at $z \sim 1.3$), we should be partially resolving its doublet shape. Therefore, also given the asymmetric profile of the observed line (J. Matthee et al. 2017; M. J. Hayes et al. 2021), it is likely to be Lyα at high redshift.

[16] https://pypeit.readthedocs.io/en/latest/

[17] The spectrum is made publicly available in Zenodo at doi:10.5281/zenodo.15306220.
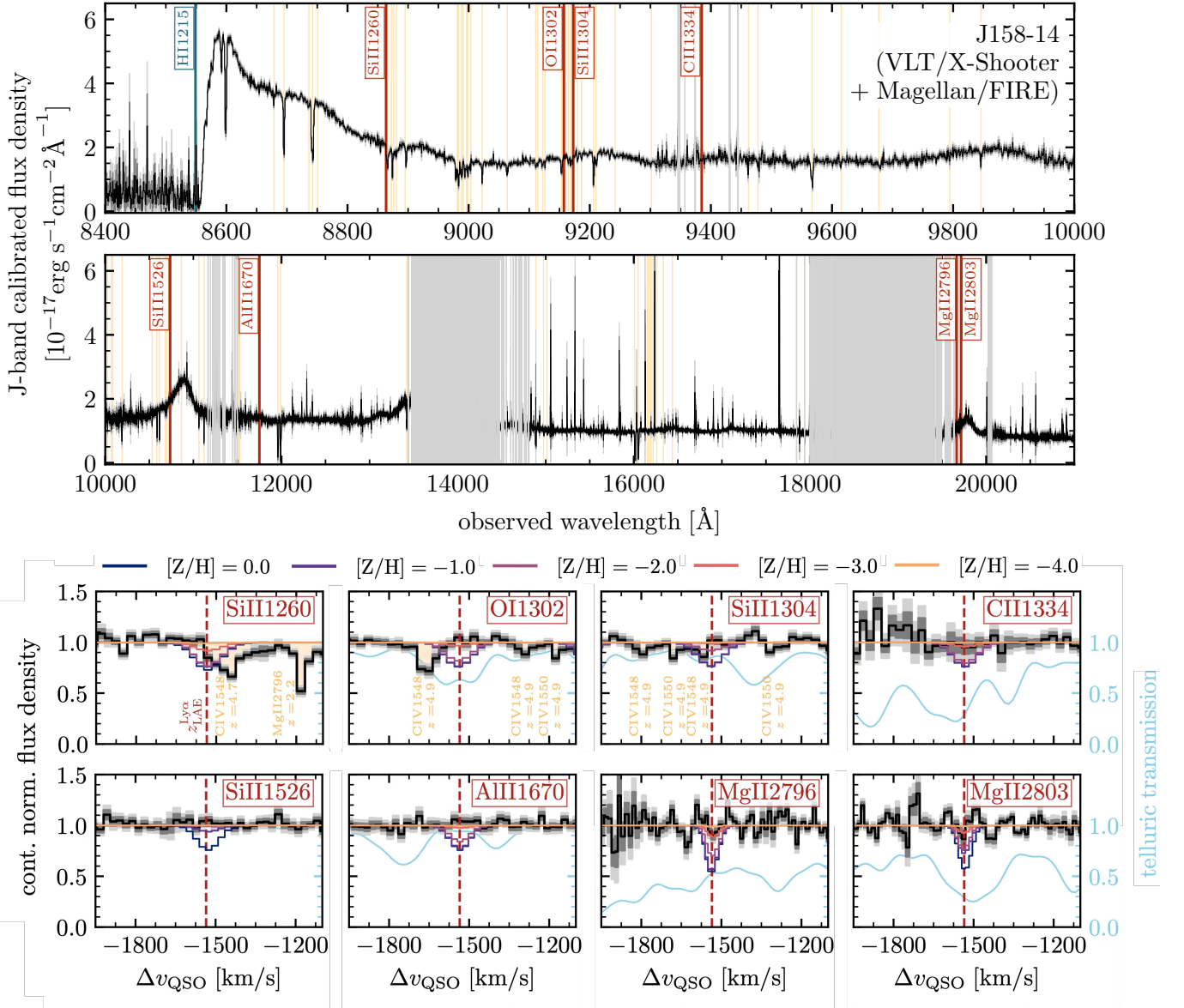
Figure 3. Top: a deep (10.2 hr) medium-resolution J-band calibrated spectrum of the quasar PSO J158-14, observed with the Magellan/FIRE and VLT/X-Shooter spectrographs. This spectrum was further continuum normalized (see the main text) and used to stack regions corresponding to low-ionization absorption lines (shown as vertical red lines) that could be associated with the foreground LAE (marked by the blue vertical line). The orange vertical lines mark all absorption lines due to foreground systems identified by R. L. Davies et al. (2023b), and the gray vertical lines mask spectral regions heavily contaminated by telluric emission. Bottom: zoom-in on the absorption line regions in the continuum-normalized spectrum that could be associated with the proximate absorber, in velocity relative to the quasar's rest frame. The dashed red line corresponds to the redshift of the LAE identified in MUSE observations, and orange regions mark absorption features due to other foreground systems (R. L. Davies et al. 2023b). Additionally, we show the telluric transmission in blue, and we overplot simulated absorption profiles at a range of metallicities [Z/H]. In both parts of the figure, the 1σ and 2σ uncertainties are shown as gray and light gray shaded regions.

After fitting the quasar spectrum shown in the top part of Figure 3 and predicting its continuum emission around Lyα following the methods in D. Ďurovčíková et al. (2020), we normalize the observed spectrum by the predicted continuum to search for metal absorption lines. We focus on regions of the continuum-normalized quasar spectrum where the accessible low-ionization metal lines at the redshift of the LAE would lie. We show these regions in the bottom part of Figure 3, with the red dashed line marking the redshift where we would expect to find absorption lines associated with this LAE. To quantify the metallicity of this LAE, we convert our estimated H I column density ($\log N_{\mathrm{HI}}/\mathrm{cm}^{-2} = 19.7$) to the column density of each atomic species assuming the solar abundance pattern (M. Asplund et al. 2009), and use the

inferred column densities to forward model individual absorption line profiles for the aforementioned transitions using the assumed broadening of this absorption system ($b = 5\,\mathrm{km\,s^{-1}}$) at a range of metal abundance ratios [Z/H]. The resultant profiles are overplotted in the bottom part of Figure 3. We also note that some of the regions are contaminated by continuum fluctuations due to sky line contamination (the telluric transmission is shown in blue).

To derive a limit on the overall metallicity and increase the SNR, we proceed by stacking the absorption line regions and their associated profiles shown in the bottom panel of Figure 3. Note that during this procedure, we mask all absorption features in the spectrum that have previously been identified as corresponding to foreground intervening absorption systems
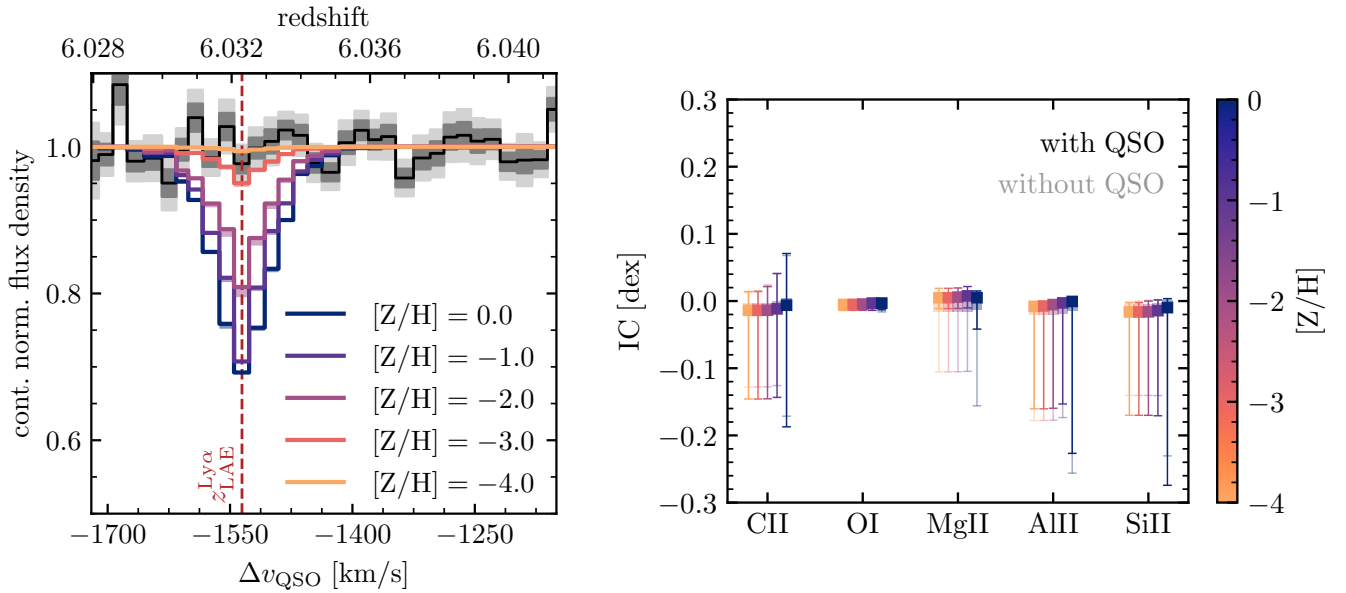
Figure 4. Left: metallicity constraint on the newly found proximate absorption system. Here we show the inverse-variance-weighted stack of low-ionization absorption line regions in the continuum-normalized spectrum of PSO J158-14, in terms of the velocity shift from the quasar's rest frame, shown in the bottom part of Figure 3, and also marked by vertical red lines in the top part of Figure 3. The 1σ and 2σ uncertainties on the stacked spectrum are shown as gray and light gray shaded regions. The modeled absorption profiles are stacked using the same weights as the data and overplotted as colored lines. There is no detectable absorption at the redshift of the LAE at this spectral resolution, yielding a metallicity constraint of $[Z/H] < -3$. This absorber thus constitutes an extremely metal-poor candidate. The shaded regions around the modeled absorption line profiles reflect the 1σ uncertainties on the ionization corrections derived from CLOUDY, as shown in the right panel. Right: ionization corrections (with 1σ uncertainties from marginalizing over the modeled hydrogen densities) to the column densities of individual ions from CLOUDY used for absorption line profile modeling. Even though this absorption system is not fully self-shielding, the corrections are close to zero. This holds even when the radiation from the background quasar is taken into account (solid data points; compared to CLOUDY models without the quasar radiation shown as semitransparent data points).

(shown as orange regions in Figure 3; R. L. Davies et al. 2023b). We show the inverse-variance-weighted mean stack in black in the left panel of Figure 4, with gray and light gray 1σ and 2σ uncertainties, respectively. The modeled absorption profiles are stacked with the same weights as the data. Note that the stacked spectrum is shown in terms of the velocity offset from the quasar; therefore, any absorption associated with the LAE would be seen at the location of the red dashed line marking $z_{\mathrm{LAE}}^{\mathrm{Ly}\alpha}$. We detect no metal absorption lines at the redshift of the LAE beyond the noise level of the stacked, high-SNR spectrum, in agreement with previous studies that used shallower data (A.-C. Eilers et al. 2020; R. L. Davies et al. 2023b).

As this system is a sub-DLA and therefore not fully self-shielding, we take into account ionization corrections (S. M. Viegas 1995) when converting the observed hydrogen column density to the column densities of the metals considered here,

$$\log N_{Z_i} = [Z/H] + \log N_{\mathrm{HI}} + \log\left(\frac{N_Z}{N_H}\right)_{\odot} - \mathrm{IC}(Z_i). \quad (1)$$

Here, $\log N_{Z_i}$ is the column density corresponding to a particular ionization state of the metal Z, $\log N_{\mathrm{HI}}$ is the column density of the neutral hydrogen (estimated from the quasar spectrum), $\log(N_Z/N_H)_{\odot}$ is the solar abundance ratio (from M. Asplund et al. 2009), and $\mathrm{IC}(Z_i)$ is the ionization correction for a given ionization state at a given metallicity.

To obtain these ionization corrections, we ran a grid of CLOUDY (v23.01; G. J. Ferland et al. 1998; M. Chatzikos et al. 2023) models at a range of metallicities, $-4.0 \leqslant [Z/H] \leqslant 0.0$ in steps of 1.0, and hydrogen densities, $-3.0 \leqslant \log n_H(\mathrm{cm}^{-3}) \leqslant 3.0$ in

steps of 0.5. We include the UV background from F. Haardt & P. Madau (2012) and the cosmic microwave background at the redshift of the LAE, as well as cosmic rays. Additionally, we include the radiation of the background quasar, as this could play a significant role in the case of this sub-DLA. The quasar's spectral energy density is modeled via the `table AGN` command normalized to a bolometric luminosity of $L_{\mathrm{bol}} = 10^{47.31}$ erg s^{-1} (A.-C. Eilers et al. 2020) and placed at a radius corresponding to the luminosity distance between the LAE and the quasar's systemic redshifts ($d_L \sim 15.9$ pMpc). We do not include the effects of dust grains as these are known to be negligible at the low metallicities most relevant to this system (A. De Cia 2018; G. Vladilo et al. 2018; A. Hamanowicz et al. 2024). From these models, we derive $\mathrm{IC}(Z_i)$ by comparing the total abundance of the element Z with respect to hydrogen to the ratio of the neutral hydrogen column density to the column density of the ionization state under consideration (S. M. Viegas 1995). Subsequently, we marginalize over the grid of modeled hydrogen densities to obtain a distribution of ionization correction for each ionic species across the different metallicities.

The derived ionization corrections are small ($\lesssim 0.3$ dex), especially at lower metallicities, even when the irradiation by the background quasar is taken into account (right panel of Figure 4; results from CLOUDY runs without the quasar radiation are shown for comparison as semitransparent data points). This is comparable to other sub-DLA corrections found in the literature (T. A. M. Berg et al. 2021; L. Welsh et al. 2024). Taking these corrections (including their 1σ uncertainties) into account yields an upper limit on the metallicity of this absorber of $[Z/H] < -3$ (left panel of Figure 4). Such a metallicity constraint implies an extremely

metal-poor absorption system in the foreground of PSO J158-14, consistent with the redshift of the foreground LAE at a projected distance of ∼29 pkpc.

3. Conclusion

Using integral field unit spectroscopy, we identified a new LAE in the immediate foreground of the quasar PSO J158-14 at $z \approx 6$ that likely represents an extremely metal-poor proximate absorption system at $[Z/H] < -3$. We detect no associated metal absorption lines in a deep, 10.2 hr medium-resolution spectrum of the quasar.

This high-redshift system is unique in that its low metallicity constraint is based on absorption spectroscopy, unlike other metal-poor galaxies identified at high-redshift with emission-line-based metallicities from JWST (E. Vanzella et al. 2023; A. J. Cameron et al. 2024; R. Maiolino et al. 2024; F. Cullen et al. 2025; S. Fujimoto et al. 2025; R. P. Naidu et al. 2025; C. J. Willott et al. 2025). The metallicity limit derived here is lower than the most metal-poor high-redshift galaxies identified to date with metallicity constraints of $[O/H] < -2.4$ (E. Vanzella et al. 2023) and $[Z/H] < -2.3$ (S. Fujimoto et al. 2025). However, it should be noted that emission and absorption line spectroscopy typically each probe different gas phases, which makes it difficult to directly compare their inferred metallicities (e.g., B. L. James et al. 2014; S. Hernandez et al. 2021).

The existence of this foreground LAE further implies that the proximity zone of the quasar is likely truncated, which in turn implies that the estimate of this quasar's lifetime based on the extent of its proximity zone is underestimated. This is supported by the fact that the MUSE data reveal a large $(24^{+24}_{-9} \text{pkpc})$ Lyα nebula around PSO J158-14 (D. Ďurovčíková et al. 2025, in preparation).

In order to confirm the redshift and the low metallicity of this absorption system, deep, high-resolution spectroscopic observations of the quasar are required to resolve such weak metal lines (as demonstrated by L. Welsh et al. 2023 in lower-redshift metal-poor DLAs). Detecting these possible absorption features would also enable us to expand this analysis beyond the assumptions of the solar abundance pattern. Additionally, at a projected distance of ∼29 pkpc, the quasar sightline is likely probing gas outside of the virial radius of this LAE, suggesting that we might be probing its circumgalactic medium that has not been enriched. Therefore, in order to confirm the low-metallicity nature of its host galaxy candidate, direct spectroscopic observations of the LAE itself are necessary. If its metallicity is confirmed, this newly detected source could prove to be the most metal-poor system currently known at high redshift and thus provide a unique opportunity to search for signatures of Pop III stars.

Acknowledgments

ORCID iDs

Dominika Ďurovčíková ⓘ https://orcid.org/0000-0001-8986-5235
Anna-Christina Eilers ⓘ https://orcid.org/0000-0003-2895-6218
Robert A. Simcoe ⓘ https://orcid.org/0000-0003-3769-9559
Louise Welsh ⓘ https://orcid.org/0000-0003-3174-7054
Romain A. Meyer ⓘ https://orcid.org/0000-0001-5492-4522
Jorryt Matthee ⓘ https://orcid.org/0000-0003-2871-127X
Emma V. Ryan-Weber ⓘ https://orcid.org/0000-0002-5360-8103
Minghao Yue ⓘ https://orcid.org/0000-0002-5367-8021
Harley Katz ⓘ https://orcid.org/0000-0003-1561-3814
Sindhu Satyavolu ⓘ https://orcid.org/0000-0001-5818-6838
George Becker ⓘ https://orcid.org/0000-0003-2344-263X
Frederick B. Davies ⓘ https://orcid.org/0000-0003-0821-3644
Emanuele Paolo Farina ⓘ https://orcid.org/0000-0002-6822-2254

References

Abel, T., Bryan, G. L., & Norman, M. L. 2002, Sci, 295, 93
Asplund, M., Grevesse, N., Sauval, A. J., & Scott, P. 2009, ARA&A, 47, 481
Bacon, R., Accardo, M., Adjali, L., et al. 2010, Proc. SPIE, 7735, 131
Bañados, E., Rauch, M., Decarli, R., et al. 2019, ApJ, 885, 59
Becker, G. D., Bolton, J. S., Zhu, Y., & Hashemi, S. 2024, MNRAS, 533, 1525
Becker, G. D., Pettini, M., Rafelski, M., et al. 2019, ApJ, 883, 163
Becker, G. D., Sargent, W. L. W., Rauch, M., & Calverley, A. P. 2011, ApJ, 735, 93
Beers, T. C., & Christlieb, N. 2005, ARA&A, 43, 531
Berg, T. A. M., Fumagalli, M., D'Odorico, V., et al. 2021, MNRAS, 502, 4009
Bosman, S. E. I., Davies, F. B., Becker, G. D., et al. 2022, MNRAS, 514, 55
Bosman, S. E. I., Fan, X., Jiang, L., et al. 2018, MNRAS,
Bromm, V. 2017, MmSAI, 88, 671
Cameron, A. J., Katz, H., Witten, C., et al. 2024, MNRAS, 534, 523
Cen, R., & Haiman, Z. 2000, ApJ, 542, L75
Chatzikos, M., Bianchi, S., Camilloni, F., et al. 2023, RMxAA, 59, 327
Chehade, B., Carnall, A. C., Shanks, T., et al. 2018, MNRAS, 478, 1649
Cooke, R., Pettini, M., Steidel, C. C., Rudie, G. C., & Nissen, P. E. 2011, MNRAS, 417, 1534
Cullen, F., Carnall, A. C., Scholte, D., et al. 2025, MNRAS, 540, 2176
Davies, F. B., Bañados, E., Hennawi, J. F., & Bosman, S. E. I. 2023a, arXiv:2312.06747
Davies, R. L., Ryan-Weber, E., D'Odorico, V., et al. 2023b, MNRAS, 521, 289
De Cia, A. 2018, A&A, 613, L2
D'Odorico, V., Banados, E., Becker, G. D., et al. 2023, MNRAS, 523, 1399
D'Odorico, V., Feruglio, C., Ferrara, A., et al. 2018, ApJ, 863, L29
D'Odorico, V., Finlator, K., Cristiani, S., et al. 2022, MNRAS, 512, 2389
Ďurovčíková, D., Eilers, A.-C., Chen, H., et al. 2024, ApJ, 969, 162
Ďurovčíková, D., Katz, H., Bosman, S. E. I., et al. 2020, MNRAS, 493, 4256
Eilers, A.-C., Davies, F. B., & Hennawi, J. F. 2018, ApJ, 864, 53
Eilers, A.-C., Hennawi, J. F., Decarli, R., et al. 2020, ApJ, 900, 37
Fan, X., Bañados, E., & Simcoe, R. A. 2023, ARA&A, 61, 373
Fan, X., Strauss, M. A., Becker, R. H., et al. 2006, AJ, 132, 117
Farina, E. P., Venemans, B. P., Decarli, R., et al. 2017, ApJ, 848, 78
Ferland, G. J., Korista, K. T., Verner, D. A., et al. 1998, PASP, 110, 761
Frebel, A., & Norris, J. E. 2015, ARA&A, 53, 631
Fujimoto, S., Naidu, R. P., Chisholm, J., et al. 2025, arXiv:2501.11678
Fumagalli, M., O'Meara, J. M., & Prochaska, J. X. 2011, Sci, 334, 1245
Fumagalli, M., O'Meara, J. M., & Prochaska, J. X. 2016, MNRAS, 455, 4100
Gunn, J. E., & Peterson, B. A. 1965, ApJ, 142, 1633
Haardt, F., & Madau, P. 2012, ApJ, 746, 125
Haiman, Z., & Cen, R. 2001, in ASP Conf. Proc. 222, The Physics of Galaxy Formation, ed. M. Umemura & H. Susa (San Francisco, CA: ASP), 101

Hamanowicz, A., Tchernyshyov, K., Roman-Duval, J., et al. 2024, ApJ, 966, 80

Hayes, M. J., Runnholm, A., Gronke, M., & Scarlata, C. 2021, ApJ, 908, 36

Heintz, K. E., Brammer, G. B., Watson, D., et al. 2025, A&A, 693, A60

Hernandez, S., Aloisi, A., James, B. L., et al. 2021, ApJ, 908, 226

Hirano, S., Hosokawa, T., Yoshida, N., Omukai, K., & Yorke, H. W. 2015, MNRAS, 448, 568

James, B. L., Aloisi, A., Heckman, T., Sohn, S. T., & Wolfe, M. A. 2014, ApJ, 795, 109

Johnson, J. L., & Aykutalp, A. 2019, ApJ, 879, 18

Katz, H., Cameron, A. J., Saxena, A., et al. 2024, arXiv:2408.03189

Katz, H., Kimm, T., Ellis, R. S., Devriendt, J., & Slyz, A. 2023, MNRAS, 524, 351

Klessen, R. S., & Glover, S. C. O. 2023, ARA&A, 61, 65

Ledoux, C., Petitjean, P., Fynbo, J. P. U., MÃýller, P., & Srianand, R. 2006, A&A, 457, 71

Madau, P., & Dickinson, M. 2014, ARA&A, 52, 415

Madau, P., & Rees, M. J. 2000, ApJ, 542, L69

Maiolino, R., Übler, H., Perna, M., et al. 2024, A&A, 687, A67

Matthee, J., Sobral, D., Darvish, B., et al. 2017, MNRAS, 472, 772

Miralda-Escudé, J. 1998, ApJ, 501, 15

Murphy, M. T., Curran, S. J., Webb, J. K., Ménager, H., & Zych, B. J. 2007, MNRAS, 376, 673

Naidu, R. P., Matthee, J., Katz, H., et al. 2025, arXiv:2503.16596

Nakajima, K., & Maiolino, R. 2022, MNRAS, 513, 5134

Planck Collaboration, Aghanim, N., Akrami, Y., et al. 2020, A&A, 641, A6

Prochaska, J. X., Hennawi, J., Cooke, R., et al. 2020a, pypeit/PypeIt: Release, v1.0.0, Zenodo, doi:10.5281/zenodo.3743493

Prochaska, J. X., Hennawi, J. F., Westfall, K. B., et al. 2020b, JOSS, 5, 2308

Ryan-Weber, E. V., Pettini, M., Madau, P., & Zych, B. J. 2009, MNRAS, 395, 1476

Saccardi, A., Salvadori, S., D'Odorico, V., et al. 2023, ApJ, 948, 35

Satyavolu, S., Eilers, A.-C., Kulkarni, G., et al. 2023, MNRAS, 522, 4918

Salvadori, S., & Ferrara, A. 2012, MNRAS: Letters, 421, L29

Sawyer, F., Bolton, J. S., Becker, G. D., et al. 2025, MNRAS, 540, 2238

Schauer, A. T. P., Drory, N., & Bromm, V. 2020, ApJ, 904, 145

Schauer, A. T. P., Glover, S. C. O., Klessen, R. S., & Ceverino, D. 2019, MNRAS, 484, 3510

Schaye, J., Aguirre, A., Kim, T.-S., et al. 2003, ApJ, 596, 768

Schindler, J.-T., Farina, E. P., Bañados, E., et al. 2020, ApJ, 905, 51

Simcoe, R. A., Burgasser, A. J., Schechter, P. L., et al. 2013, PASP, 125, 270

Simcoe, R. A., Onoue, M., Eilers, A.-C., et al. 2020, arXiv:2011.10582

Simcoe, R. A., Sargent, W. L. W., & Rauch, M. 2002, ApJ, 578, 737

Simcoe, R. A., Sullivan, P. W., Cooksey, K. L., et al. 2012, Natur, 492, 79

Sodini, A., D'Odorico, V., Salvadori, S., et al. 2024, A&A, 687, A314

Spina, B., Bosman, S. E. I., Davies, F. B., Gaikwad, P., & Zhu, Y. 2024, A&A, 688, L26

Tornatore, L., Ferrara, A., & Schneider, R. 2007, MNRAS, 382, 945

Vanni, I., Salvadori, S., D'Odorico, V., Becker, G. D., & Cupani, G. 2024, ApJ, 967, L22

Vanzella, E., Loiacono, F., Bergamini, P., et al. 2023, A&A, 678, A173

Vernet, J., Dekker, H., D'Odorico, S., et al. 2011, A&A, 536, A105

Viegas, S. M. 1995, MNRAS, 276, 268

Vladilo, G., Gioannini, L., Matteucci, F., & Palla, M. 2018, ApJ, 868, 127

Wang, F., Davies, F. B., Yang, J., et al. 2020, ApJ, 896, 23

Weilbacher, P. M., Streicher, O., Urrutia, T., et al. 2012, Proc. SPIE, 8451, 84510B

Weilbacher, P. M., Streicher, O., Urrutia, T., et al. 2014, in ASP Conf. Ser 485, Astronomical Data Analysis Software and Systems XXIII, ed. N. Manset & P. Forshay (San Francisco, CA: ASP), 451

Welsh, L., Cooke, R., Fumagalli, M., & Pettini, M. 2023, MNRAS, 525, 527

Welsh, L., Cooke, R., Fumagalli, M., Pettini, M., & Rudie, G. C. 2024, A&A, 691, A285

Willott, C. J., Asada, Y., Iyer, K. G., et al. 2025, arXiv:2502.07733

Yang, J., Wang, F., Fan, X., et al. 2020, ApJ, 904, 26

Yue, M., Eilers, A.-C., Simcoe, R. A., et al. 2023, ApJ, 950, 105

Zhu, Y., Becker, G. D., Bosman, S. E. I., et al. 2024, MNRAS, 533, L49